Chemical Science

EDGE ARTICLE

View Article Online
View Journal | View Issue

Cite this: *Chem. Sci.*, 2017, **8**, 2365

Rectification of current responds to incorporation of fullerenes into mixed-monolayers of alkanethiolates in tunneling junctions†

Li Qiu, Yanxi Zhang, Theodorus L. Krijger, Xinkai Qiu, Patrick van't Hof, Jan C. Hummelen and Ryan C. Chiechi*

Received 28th October 2016
Accepted 18th December 2016

DOI: 10.1039/c6sc04799h

www.rsc.org/chemicalscience

This paper describes the rectification of current through molecular junctions comprising self-assembled monolayers of decanethiolate through the incorporation of C_{60} fullerene moieties bearing undecanethiol groups in junctions using eutectic Ga–In (EGaIn) and Au conducting probe AFM (CP-AFM) top-contacts. The degree of rectification increases with increasing exposure of the decanethiolate monolayers to the fullerene moieties, going through a maximum after 24 h. We ascribe this observation to the resulting mixed-monolayer achieving an optimal packing density of fullerene cages sitting above the alkane monolayer. Thus, the degree of rectification is controlled by the amount of fullerene present in the mixed-monolayer. The voltage dependence of R varies with the composition of the top-contact and the force applied to the junction and the energy of the lowest unoccupied π-state determined from photoelectron spectroscopy is consistent with the direction of rectification. The maximum value of rectification $R = |J(+)/J(-)| = 940$ at ±1 V or 617 at ±0.95 V is in agreement with previous studies on pure monolayers relating the degree of rectification to the volume of the head-group on which the frontier orbitals are localized.

1 Introduction

Molecular rectification is the asymmetric current response to an external voltage bias of equal magnitude but opposite sign mediated by the electronic structure of individual molecules. In contrast to comparisons of current (I) or current-density (J), rectification has the advantage that it is self-referencing, which eliminates the resistance of the contacts in studies comparing the electronic structure of molecular tunneling junctions. Molecular diodes are, therefore, interesting both for functionality and fundamental, phenomenological study. Rectification can be controlled to some degree by tailoring molecules and/or altering the contacts.[1–23] While the details of the mechanism can vary between experimental platforms, Nijhuis and co-workers have elucidated it unambiguously for $Ag^{TS}/S(CH_2)_{11}Fc//Ga_2O_3/EGaIn$ junctions, where EGaIn is eutectic GaIn alloy[24,25] and Fc is either ferrocene or biferrocene incorporated into a self-assembled monolayer (SAM) supported by template-stripped Ag (Ag^{TS}) and '/' and '//' denote covalent and non-covalent interfaces, respectively.[26–32] Depending on the sign of the applied bias, the difference in energy between the Fermi level (E_f) and the highest-occupied π-state (HOPS) of the Fc increases or decreases, increasing or decreasing the relative rate of charge-transfer.[33,34]

Yoon and Whitesides have shown rectification that is mediated instead by the lowest-unoccupied π-state (LUPS) of bipyridine (Bp) and naphthoquinone (Nq) moieties in $Ag^{TS}/S(CH_2)_{11}B_p//Ga_2O_3/EGaIn$ junctions, though the degree of rectification was significantly lower in the latter.[29,35] In these junctions, the sign of the applied bias at which the current is higher is reversed compared to Fc because E_f lies closer to the LUPS than the HOPS. In both cases, the magnitude of rectification, defined as $R = |J(+V)/J(-V)|$ (measured at ±1 V) depends both on the structure of the SAM and on the volume of the π-system (*i.e.*, Fc or Bp), thus it can be tuned by altering the substrate[36] or through dilution with disulfides (to introduce defects)[37] or non-rectifying alkanethiols[38] and, in principle, by increasing the size of the π-system.[27,39] These studies demonstrated a decrease in R either through the introduction of defects into the substrate or by introducing non-rectifying (or defect-inducing) compounds into the solution from which the SAMs were formed, establishing the sensitivity of R to the packing of the π-systems that mitigates rectification.

Fullerenes, due to their spherical geometry and unique optical and electronic properties, are widely studied for potential applications ranging from sensors and photovoltaic cells to nanostructured devices.[40–43] Their high affinity for noble metals and large surface area available for contact also make them

Stratingh Institute for Chemistry, Zernike Institute for Advanced Materials, University of Groningen, Nijenborgh 4, 9747 AG Groningen, The Netherlands. E-mail: r.c.chiechi@rug.nl

† Electronic supplementary information (ESI) available. See DOI: 10.1039/c6sc04799h

attractive candidates for applications in Molecular Electronics (ME), both in single-molecule (*e.g.*, break-junctions) and large-area (*e.g.*, EGaIn) platforms. Fullerene-based anchoring groups have been demonstrated in single-molecule junctions[44,45] and in large-area junctions[46] and several studies on functionalized fullerene-based SAMs have shown that the electronic structure of [60]fullerene (C_{60}) remains intact even when the carbon cages are confined to a surface.[46–48] Thus, the low-lying lowest-unoccupied molecular orbital (LUMO) of C_{60} (−4.5 eV)[49] should translate into an accessible LUPS in SAM-based junctions and, therefore, rectification *via*, the mechanism described above. The large volume and spherical symmetry of C_{60} should lead to large magnitudes of $\log|R|$ and decreased sensitivity to packing/ordering compared to Bp.

We functionalized C_{60} with 11-unedecanethiol (**SC11**) to afford **FSC11** (structure and synthetic detail shown in Fig. S1 in ESI† and corresponding thiolate shown in Fig. 2A) and compared the J/V characteristics of Ag^{TS}/**FSC11**//Ga_2O_3/EGaIn junctions to those reported for junctions comprising SAMs of Fc and Bp functionalized with **SC11**. We prepared the SAMs of **FSC11** by incubating SAMs of 10-dodecanethiol (**SC10**) with **FSC11**, observing an increase in R with exposure time. This method of preparing mixed-monolayers prevents phase-segregation between the two dissimilar compounds and preserves the packing of the SAM. Thus, the magnitude of R corresponds to the degree of incorporation of **FSC11** into the non-rectifying SAM of **SC10** and not a change in packing or an increase in disorder. We ascribe the rectification of current to the LUPS-mediated mechanism described above, which is summarized in Fig. 1.

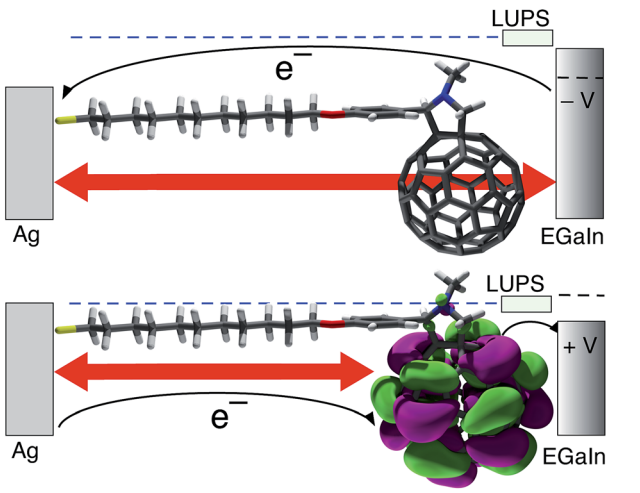

Fig. 1 A schematic showing the mechanism of rectification. At negative bias (top) the lowest-unoccupied π-state (LUPS; indicated by a light green rectangle) is pushed out of resonance with the Ag electrode as is depicted by the blue dashed line. The width of the tunneling barrier (indicated with a double-headed red arrow) is therefore defined by the entire end-to-end length of the molecule and electrons must tunnel through the entire physical width of the junction. At positive bias (bottom) the LUMO (visualized as purple and green isosurfaces) is brought into resonance with the Ag electrode and electrons can tunnel to the LUPS, which is localized entirely on the C_{60} cage, and then hop to EGaIn. The width of the tunneling barrier is therefore defined only by the aliphatic portion of FSC11, thus electrons must tunnel through a distance approximately equal to SC10.

2 Results and discussion

The preparation of SAMs of fullerene derivatives functionalized with thiols on metal surfaces has been extensively studied.[50–56] Contrary to simple systems such as alkanethiols, the self-assembly of fullerene derivatives on gold is complicated by the formation of multilayers and head-to-tail assemblies due to competition from the strong fullerene–fullerene and fullerene–gold interactions.[54,57–60] (The same complexities are expected on Ag.) These problems can be mitigated by pre-passivating the substrate with a SAM of decanethiol (**SC10**) and then forming a mixed-monolayer by incubating this SAM in a solution containing the fullerene derivatives (see Experimental).[47,61] Throughout this manuscript we refer to mixed-monolayers of **FSC11** and **SC10** prepared by this method simply as SAMs of **FSC11** unless specified otherwise.

We measured the J/V characteristics of Ag^{TS}/**FSC11**//Ga_2O_3/EGaIn and Au^{TS}/**FSC11**//Ga_2O_3/EGaIn junctions (Fig. 2A) by acquiring 1016 (650 on Ag and 366 on Au) sweeps between ±0.5 V for 61 (37 on Ag and 24 on Au) junctions across 7 (4 on Ag and 3 on Au) substrates (Table 1). The frequency of shorts increased dramatically above 0.5 V precluding the extraction of meaningful statistics above 0.5 V. We also measured Ag^{TS}/SAM//Ga_2O_3/EGaIn junctions based on SAMs of pure **FSC11** and **SC10** for comparison. We calculated R by dividing each value of J at positive bias into the corresponding value at negative bias for each value of $|V|$ and then fitting a Gaussian to the resulting histogram of $\log|R|$ and expressing the error as the confidence interval of the fit. Histograms comparing $\log|R|$ for SAMs of pure **FSC11** and mixed-monolayers of **FSC11** SAMs on Ag^{TS} are shown in the ESI.† Although both monolayers show comparable peak values of $\log|R|$, the histogram of the pure SAM is broad and possibly multi-modal, while that of the mixed-monolayer is a single, log-normal distribution. We ascribe this difference to the strong fullerene–metal interactions competing with thiol–metal interactions to form mixed phases of upright (thiol-down) and upside-down (fullerene-down) molecules. Despite these differences, the yields of working junctions for the pure SAMs of **FSC11** *versus* the mixed-monolayers are comparable (Table 1), which underscores the utility of using statistics and observables such as $\log|R|$ to characterize tunneling junctions comprising SAMs.

Fig. 2B shows the J/V curves of the junctions before and after exchanging **FSC11** into the passivating SAM of **SC10** as described above (see ESI† for details of the data acquisition and processing). The J/V curve of **SC10** is almost perfectly symmetric ($\log|R| = 0.07$), reaching a maximum of $\log|J| \approx -1$ at ±0.5 V (the units of J throughout this paper are A cm^{-2}). After exchange, however, the maximum value of $\log|J|$ at −0.5 V drops below −3, while the value at +0.5 V remains almost equal to that of **SC10**. This asymmetry results in a value of $\log|R| = 1.46 \pm 0.018$ and is characterized by a suppression of leakage current (at negative bias) compared to the SAM of pure **SC10** caused by the increase in tunneling distance imposed by the C_{60} cage

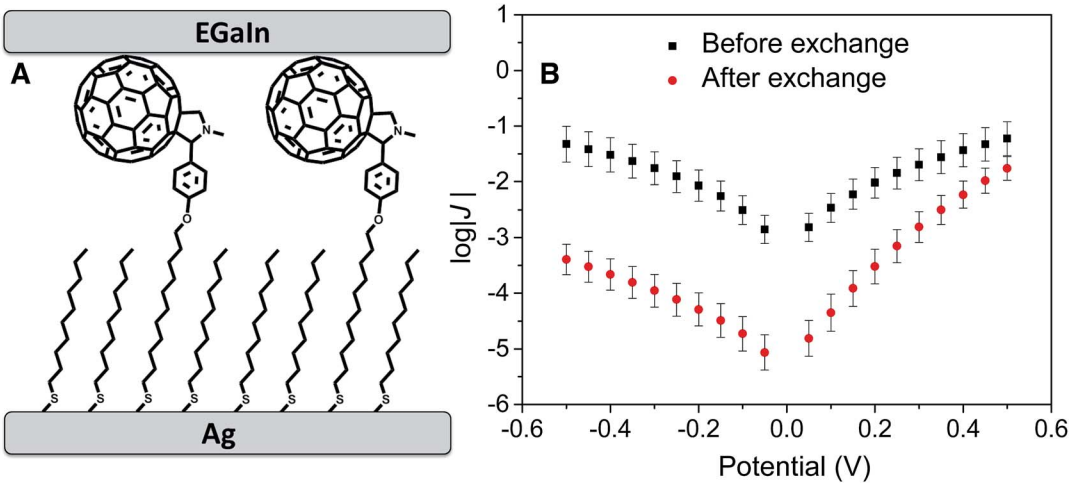

Fig. 2 (A) Schematic diagram of a Ag^{TS}/**FSC11**//Ga_2O_3/EGaIn junction prepared by incubating a SAM of **SC10** on Ag^{TS} in a solution of **FSC11**. (B) Plots of log|*J*| (the units of *J* are A cm^{-2}) *versus V* for SAMs of **SC10** on Ag^{TS} before and after incubation with **FSC11**. Each datapoint is the mean from a Gaussian fit to a histogram of log|*J*| for that value of *V* (see ESI† for details) and the error bars are the 95% confidence intervals of the fit. The *J*/*V* of **SC10** is symmetric, with a maximum value of log|*J*| of approximately −1. After exchanging **FSC11** into this SAM, log|*J*| decreases by approximately 2 at negative bias, giving rise to rectification. The magnitude of *J* at 0.5 V is almost identical before and after exchange because the width of the tunneling barrier at positive bias is nearly equal (see Fig. 1).

Table 1 Statistics for the measured junctions

SAM	Substrates	Junctions	Traces	Unstable[a] (%)	Yield[b] (%)	*R*@±0.5 V
Ag^{TS}/**FSC11**	4	42	650	5 (12)	88	29 ± 1
Ag^{TS}/**SC10**	1	8	166	0	100	1
Au^{TS}/**FSC11**	3	28	366	4 (14)	86	8 ± 1
Ag^{TS}/**FSC11**[c]	3	25	25	24 (96)[d]	4	617[e]
Ag^{TS}/**FSC11**[f]	3	34	568	3 (9)	91	43 ± 9

[a] Junctions with noisy *J*/*V* curves that shorted readily. [b] Non-shorting junctions that gave smooth *J*/*V* curves. [c] Measurement was conducted at ±1 V. [d] The low yield is due to the high bias. [e] The value was obtained for the highest one at ±0.95 V. [f] Junction comprising pure SAMs formed directly from **FSC11**.

(Fig. 1). At positive bias, the LUPS is sufficiently close to E_f of the Ag electrode that electron transport is mediated by the LUPS of the C_{60} cage and tunneling occurs only through the aliphatic portion of the SAM followed by hopping between C_{60} cage and EGaIn. Hence the magnitude of *J* is nearly equal for SAMs of **SC10** and **FSC11** at +0.5 V.

Ferrocene-based rectifiers exhibit a strong odd–even effect in the magnitude of log|*R*| caused by the angle of the ferrocenes differing for even- and odd-numbered alkyl spacers.[30,62,63] The observation of this effect provides compelling evidence that rectification is indeed caused by interactions between the ferrocene and the EGaIn electrode. The spherical symmetry of C_{60} precludes such a study for **FSC11**, however, varying the length of the alkanethiolates into which **FSC11** is exchanged should have no influence on tunneling transport if it is indeed mediated by the C_{60} group. Fig. S9† shows the *J*/*V* curves of mixed-monolayers of **FSC11** exchanged into SAMs of **SC8**, **SC10** and **SC12**; they are nearly identical, giving both the same magnitudes of log|*J*| and log|*R*| and supporting the hypothesis that tunneling currents are mediated entirely by **FSC11** in mixed-monolayers.

To exclude the possibility that the increase in log|*R*| after exposure of **SC10** to **FSC11** is due to electrochemical reactions between the Ag^{TS} electrode and the C_{60} cage, we measured Au^{TS}/**FSC11**//Ga_2O_3/EGaIn junctions where Au^{TS} is template-stripped Au prepared identically to Ag^{TS}. The lower work function of Au^{TS} compared to Ag^{TS} has two potential consequences on log|*R*|: (i) the rectification of current is due to redox reactions taking place at the Ag^{TS} electrode, which will be pushed out of the experimental bias window; (ii) the lower (more negative) E_f of Au^{TS} will increase the bias required to move the LUPS of **FSC11** close enough to resonance to induce rectification. The corresponding observables are log|*R*| ≈ 1 (i) and a decrease in log|*R*| at ±0.5V (ii). We observe the latter: log|*R*| decreases from 1.46 ± 0.018 on Ag^{TS} to 0.92 ± 0.017 on Au^{TS} from which we conclude that the origin of rectification in mixed SAMs of **FSC11**/**SC10** is indeed the onset of a hopping as the LUPS comes close to E_f and not electrochemistry at the Ag^{TS}.

To support this conclusion, we compared the LUPS energies of SAMs of **FSC11** and Bp and Nq using a combination of optical and photoelectron spectroscopy. The LUPS of **FSC11** is approximately 3.72 eV (see ESI†), which is nearly identical to Bp

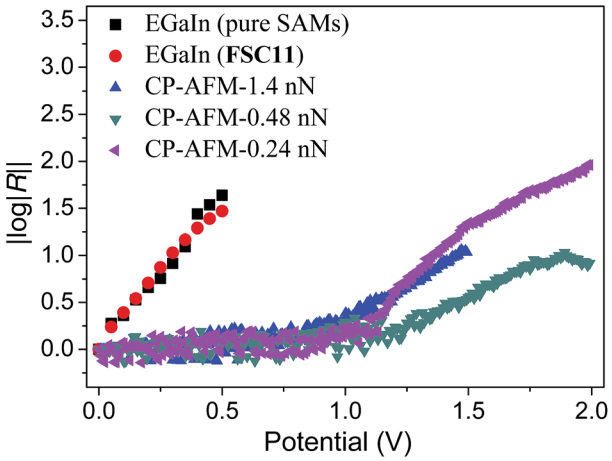

Fig. 3 Comparison of log|*R*|–|*V*| plots of EGaIn (black squares and red dots) and CP-AFM (blue, green and magenta symbols) measurements. The Gaussian mean values for junctions based on pure and mixed **FSC11** SAMs from EGaIn measurements show an identical trend, however, the variance (shown in the ESI†) is much higher for the pure SAMs. CP-AFM measurements gave values of log|*R*| > 1 at loading forces of 0.24 nN, 0.48 nN and 1.4 nN, but with opposite polarity from that of EGaIn due to the difference in wiring (as is described in ref. 65). The original curves with error bars are shown in ESI.† The onset of rectification occurs are at higher bias (2 V and 1.5 V) for CP-AFM than (0.5 V) for EGaIn, at least some of which is due to the low-current detection limit of CP-AFM at low bias.

(3.7 eV)[38] and Nq (3.9 eV)[29] and close to the assumed E_f of Ga_2O_3/EGaIn electrode (approximately 4.3 eV). Thus, it is plausible that the mechanism of rectification for **FSC11** is the same as Bp since the electrodes and substrates are identical. We also measured the *I*|*V* characteristics of SAMs of **FSC11** using conductive probe atomic force microscopy (CP-AFM)[64] which replaces a conformal, liquid-metal electrode (EGaIn) with a rigid Au electrode. Fig. 3 compares log|*R*| as a function of voltage for Ag^{TS}/**FSC11**//EGaIn and Ag^{TS}/**FSC11**//Au. (Note that the wiring is reversed, thus we use the convention of EGaIn junctions to express log|*R*| as we have done previously.[65]) Interestingly, log|*R*| rises much faster with EGaIn, crossing 1.0 only above ±1.25 V with CP-AFM. The sudden onset with CP-AFM is due to the low-current limit (our CP-AFM module uses fixed op-amps, unlike our EGaIn setup) clipping data at low bias. Nonetheless, there is a significant difference between the values of *V* at which the magnitude of log|*R*| is equal between CP-AFM and EGaIn. This result suggests that both electrodes—that is, E_f or their mechanical properties—play an important role in the magnitude of rectification. The weaker dependence on bias for CP-AFM could simply be due to weaker coupling at the SAM//Au interface, such that the offset between E_f and the LUPS is higher for a particular voltage with CP-AFM compared to EGaIn. Changing the loading force of the AFM tip does change the magnitude of log|*R*|, but the onset of rectification is approximately 1 V higher than it is for EGaIn top-contacts. This result suggests that the different behavior is due to the difference in work function between EGaIn and Au and/or that conformal EGaIn contacts couple much more effectively to the SAM. Whatever the origins of the difference, log|*R*| is greater than 1 in both cases, meaning that the origin of rectification is the electronic structure of the SAM and not Ag^{TS} or EGaIn.[29]

An interesting consequence of using log|*R*| as an observable is that the dynamics of the exchange between **FSC11** and the passivating SAM of **SC10** by observing the evolution of log|*R*| in time. (Assuming the magnitude of log *R* corresponds directly to the amount of **FSC11** incorporated into the SAM.) Fig. 4 shows log|*R*| *versus* exchange time (the amount of time a SAM of **SC10** was exposed to a solution of **FSC11**). Following a relatively rapid increase, log|*R*| saturates after 24 h, implying that the mixed-monolayer reaches an equilibrium structure past which it becomes energetically unfavorable to incorporate any more **FSC11**. We interpret this saturation as the point at which the fullerene head-groups (which rise above the SAM of **SC10**) have reached maximum packing density as is depicted in Fig. 2A. We recently observed similar kinetics by following the on/off ratio of SAMs of spiropyran switches as a function of exposure time to hexanethiol.[66] This timescale is also normal for place-exchange between adsorbed thiolates.[67,68] Thus, EGaIn can be used to follow the dynamics of exchange in mixed-monolayers by observing the changing characteristics of the commensurate tunneling junctions.

If **FSC11** does indeed rectify current *via* the mechanism described above, the maximum observed rectification should relate to the volume of the C_{60} cage because the LUPS is localized to the C_{60} π-system that is in contact with and (partially) pinned to the Ga_2O_3/EGaIn electrode. As is hypothesized for Bp, positive bias decreases E_f (relative to vacuum) at that electrode, which also decreases the LUPS and brings it into resonance with E_f at the Ag^{TS} electrode. At this point the LUPS becomes energetically accessible and charges tunnel from Ag^{TS} onto the C_{60} cage instead from Ag^{TS} to Ga_2O_3/EGaIn (or Au in the case of CP-AFM). Assuming a rectangular tunneling barrier, $J = J_0 \exp(-\beta d)$ where β is the tunneling decay coefficient, d is the barrier width and J_0 is the extrapolated value of J when $d = 0$. Using this equation we can estimate log|*R*| by calculating J using the value of d corresponding to the end-to-end lengths of

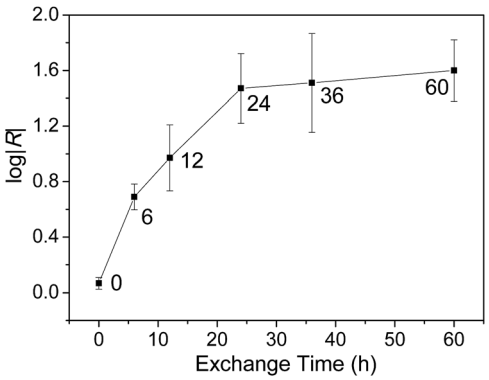

Fig. 4 A plot of log|*R*| *versus* the time that SAMs of **SC10** were exposed to solutions of **FSC11** (exchange time) using EGaIn top-contacts. The magnitude of log|*R*| increases gradually, saturating above 24 h, indicating the nearly complete **FSC11** SAM was achieved after 24 h. The values of log|*R*| and the error bars are the mean and standard deviation from Gaussian fits to histograms of *R* for each value of *V*.

Table 2 Summary of calculated molecular lengths (d) and rectification ratios (R) for **FSC11**, Bp and Fc

Assumed structure of T group	Molecular rectifiers	d_{RM} (Å)	Rectification ratio (R) Calcd[c] ($\beta \sim 0.6$ Å^{-1})	Obsd
Spherical shape	**FSC11**[a]	10.9	692	940
	Bp[b]	6.8	59	85
	Fc	7.2	73	150
Extended *trans* structure	**FSC11**	11.2	829	940
	Bp	7.2	75	85
	Fc	6.0	36	150

[a] Calculations for **FSC11** were based on the assumptions that either (i) the terminal group, which we treated as the molecular moiety excluding only the aliphatic spacer, is spherical in shape, and the width of tunneling barrier of terminal group is $d_{RM} = 2 \times (3/4\pi)^3$; or (ii) that the terminal group is an extended *trans* structure. [b] Numbers for Bp and Fc were taken from ref. 35. [c] Values of $|R|_{calcd}$ were calculated with equation $|R|_{calcd} = \exp(\beta_{RM} d_{RM})$, assuming that the tunneling decay constants characteristic of attenuation through **FSC11**, Bp and Fc are equal to that of oligophenylenes ($\beta \sim 0.6$).

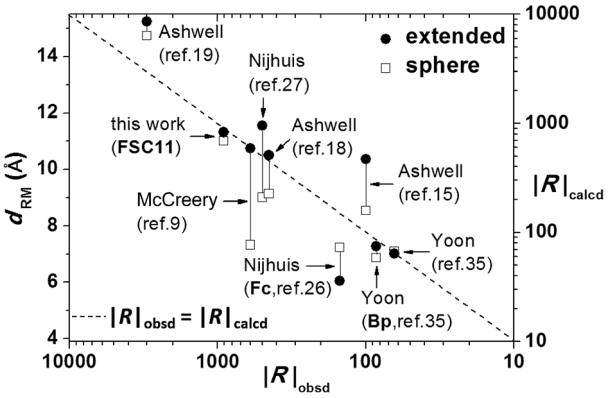

Fig. 6 A comparison of the observed and predicted magnitudes of rectification $|R|$ at ±1 V based on the volume of the π-system confined to the head-group for **FSC11** and other systems from the literatures following the methodology of ref. 35. The experimental value of $|R|$ for **FSC11** is the maximum value observed only in a few hero junctions. The two different methods of calculating volume give very similar values for **FSC11** because of its spherical geometry.

FSC11 and d_{CH_2} corresponding that value with the volume of the LUPS removed (that is, the red arrows in Fig. 1). This methodology in turn allows a direct comparison to Bp.[35] The results are summarized in Table 2.

We first calculated d_{RM} (the width of the tunneling barrier for the rectifying moiety) based on two different approximations used in ref. 35 to be 10.9 Å for a spherical volume and 11.2 Å for the volume of an extended structure, respectively. Not surprisingly, the two different methods of calculating volume give very similar values for **FSC11** because the C_{60} cage is nearly spherical. To compare observed values of rectification it is necessary to pick a value of $|V|$ at which to compute $|R|_{obsd}$. Thus far we have used ±0.5 V because the junctions were not sufficiently stable above this value to collect sufficient data for a robust statistical analysis. However, the standard value in ME is ±1.0 V. Fig. 5 shows a linear dependence of $\log|R|$ on $|V|$ from which we extrapolated a value of $R = 676$ at ±0.95 V. We compared this value to $R = 617$ from a 'hero junction' that survived sweeping to ±0.95 V (which most junctions did not) and gave qualitatively similar curves to the more robust and reproducible curves acquired at ±0.5 V. This very close agreement and the fact that plots of $\log|R|$ *versus* $|V|$ for SAMs of **FSC11** at different exchange time (24, 36 and 60 h) gave the same slope (see ESI†) validates the extrapolated value of $|R|_{obsd} = 940$ at ±1.0 V. Fig. 6 compares values of $|R|_{obsd}$ and $|R|_{calcd}$ to several other rectifiers, including Fc and Bp; **FSC11** lies almost exactly on the diagonal, further validating the presumed mechanism.

3 Conclusions

We have shown that **FSC11** SAMs composed of decanethiolate (**SC10**) and functionalized C_{60} bearing undecanethiol groups (**FSC11**) reproducibly rectify current in Ag^{TS}/SAM//EGaIn

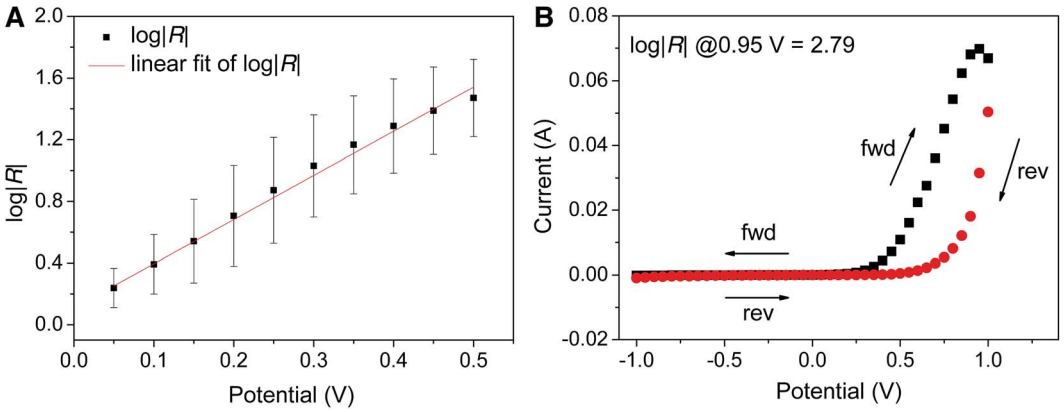

Fig. 5 (A) Linear fit of $\log|R|$ *vs.* $|V|$ of **FSC11** with EGaIn as a top-contact. The data and error bars are the mean and standard deviations of Gaussian fits (adjusted R-square = 0.994) (B) $I|V$ data for a representative 'hero' junction (which could survive sweeping to a voltage bias higher than ±0.5 V) that produce stable $I|V$ curves above 0.5 V showing a typical degree of hysteresis and a maximum value of $\log|R|$ of 2.79.

junctions at ±0.5 V. The mechanism is identical to those of SAMs containing bipyridyl (Bp) and Nq since the LUMO of these compounds lie at nearly the same energy, translating into an accessible π-state in SAM-based junctions under positive bias. Further, we show unambiguously that rectification is the result of the electronic structure of C_{60} because it persists with Au^{TS} bottom electrode and with Au top-contact. We circumvented the difficulties of growing SAMs from C_{60} derivatives by preparing mixed-monolayers *via* exchange into substrates pre-passivated with SAMs of **SC10** such that the C_{60} cages are never exposed to bare metal surfaces.

Among the molecular rectifiers included in Fig. 6, the fullerene head group of **FSC11** is the second largest behind the copper phthalocyanine salt complex from ref. 19 measured by scanning tunneling microscopy (STM). Not only does **FSC11** show the second-highest magnitude of rectification, it shows rectifying behavior with a large-area, conformal EGaIn top-contact and a nanoscopic, rigid Au top-contact. Moreover, the spherical symmetry of C_{60} and the use of mixed-monolayers mitigates the extreme sensitivity of molecular rectifiers to the details of packing and supramolecular structure. The magnitude of rectification for ferrocene moieties, for example, is sensitive to tilt angle[30] and the purity of the thiol-precursor is also crucial; less than 5% of disulfide disrupts the packing and causes a drop in R and rectification vanishes completely at 15%.[37] Similarly, forming mixed monolayers of Bp with *n*-alkanethiolates only decreases R from that of pure Bp and phase separation makes binary SAMs with relatively uniform composition difficult to achieve.[38] Since we begin from non-rectifying SAMs of **SC10** into which **FSC11** is incorporated, R increases to a saturation point.

The magnitude of $\log|R|$ at ±0.5 V is 1.46 ± 0.018, which can reach as high as 940 at ±1 V in a few hero junctions (too few for statistical analysis). This value (940) is consistent with calculations assuming the proposed rectification mechanism, further supporting the proposed relationship between the volume and energy of the accessible π-state and the magnitude and direction of rectification. Future work will focus on stabilizing junctions containing C_{60} above ±1 V to utilize the large magnitude of rectification in the hero junctions in device platforms.

4 Experimental section

Materials

11-Bromoundec-1-ene, 4-hydroxybenzaldehyde, thioacetic acid, 1-decanethiol (**SC10**) were obtained from Sigma-Aldrich and used as received with the exception of **SC10** which was purified by column chromatography (silica, hexane). The C_{60} used for the synthesis was of 99.5% purity (purchased from Solenne BV, Groningen, the Netherlands). All compounds were stored in nitrogen-flushed vials and in the dark. Their structures were verified by acquiring ^{1}H-NMR and IR spectra immediately prior to use and comparing to the spectra acquired immediately after purification. **FSC11** was prepared starting from 11-bromoundec-1-ene as described in the ESI.† All new compounds were all fully characterized by means of HRMS, NMR and IR. The Ag^{TS} and Au^{TS} substrates used in this work were made by mechanic template stripping as described elsewhere;[21] we deposited 200 nm of Ag and 100 nm of Au (99.99%), respectively, by thermal vacuum deposition onto a 3″ silicon wafer (with no-adhesion layer). Using the UV-curable optical adhesive (OA) Norland 61, we glued 1 cm^2 glass chips on the metal surfaces.

SAM formation

SAMs of **FSC11** were prepared through exchange of **SC10** from its SAMs with **FSC11** through two steps. Firstly, SAMs of **SC10** were formed by incubating freshly cleaved 1 × 1 cm^2 Ag^{TS} surfaces for 24 h in 2 mL of 2 mM solution of **SC10** in degassed ethanol (100%; anhydrous) at room temperature. The substrates were then rinsed gently with 200 proof ethanol (3 × 1 mL) and residual solvent on surface was removed by gently blowing N_2. SAMs of **FSC11** were then prepared by incubation of the resulting SAMs of **SC10** (bared Ag^{TS} surfaces used directly for the pure SAMs) in 0.5 mM solutions of **FSC11** in degassed toluene at room temperature for 24 h. After incubation, they were then rinsed with toluene and dried as previously described and then used for the measurements.

SAM characterization: contact angle measurement

The SAM of **FSC11** was first evaluated with water contact angle measurements under ambient conditions on a SCA20 Data Physics instrument with software version 3.60.2. Equilibrium contact angles were obtained by applying 1 μL water droplets on SAMs using the sessile drop method. The contact angle was measured at three different locations on each surface and the results were averaged. The results showed an average contact angle of 68 ± 1°, which corresponds closely to values of C_{60}-SAM reported by Tsukruk and co-workers.[69] While, before the exchanging, the SAM of **SC10** was determined to be more hydrophobic with a contact angle of 94 ± 1°, which also confirmed the formation of the fullerene SAM. See ESI† for a description of the EGaIn measurement setup.

XPS thickness measurement

To measure the thickness of the SAM, XPS measurements were performed using a VG Microtech spectrometer with a hemispherical electron analyzer (Clam 100), and a MgKα (1253.6 eV) X-ray source. The $Ag_{3p3/2}$ and Ag_{3d} peaks were acquired with the sample rotated under 0, 10, 20, 30, 40, and 50 degrees with respect to the electron analyzer. A Gaussian fit with background was made to the peaks to obtain their intensities. To correct for slow fluctuations in the X-ray source intensity we acquired the spectra for each peak at 0° in between the measurements where the sample is rotated. These measurements are used to obtain a correction factor γ_I.

The corrected peak intensities I^* are given by $I^* = \gamma_I I$ and can be used to determine the thickness of the layer. The values are given in ESI.† The measured electrons in the peaks are the electrons that make it from the silver through the layer without scattering. An expression for the intensity of the peaks for different lengths of the path that through the overlayer:

$$I(\phi) = I_0 \exp\left(\frac{-L}{\lambda}\right) = I_0 \exp\left(\frac{-d}{\lambda \cos(\phi)}\right), \quad (1)$$

with L the length of the path through the layer, d the thickness of the layer, λ the inelastic mean free path, and ϕ the angle of rotation of the sample with respect to the analyzer. λ depends on the kinetic energy of the observed electrons and the material the electrons have to move through. We have determined the values of λ, for electrons originating from the Ag_{3d} and Ag_{3p} levels, from measurements on a SAM of **SC10** on silver, whose thickness was well studied ((12 ± 3) Å).[70] The values were found to be 8 $Å^{-1}$ and 8.8 $Å^{-1}$ for Ag_{3d} and Ag_{3p} respectively. With these values of λ we can make a fit to the corrected intensities to find the thickness of the **FSC11** SAM, which was found to be $d = 1.8 \pm 0.3$ nm. This treatment assumes the inelastic mean free path in the **FSC11** SAM to be equal to that in the **SC10** SAM. The lower packing density of **FSC11** could lead to a slight underestimation of the thickness of the layer.

Estimation of LUMO of FSC11

The UV-vis absorption spectrum of **FSC11** enables the estimation of optical band gap (E_g) to be 1.73 eV from the onset wavelength of 718.13 nm. Ultraviolet photoelectron spectroscopy (UPS) analysis of the SAM-bound Ag^{TS} (Ag^{TS}/SC11P) for estimating the Fermi level of the silver, and the HOMO level of the **FSC11** relative to the Fermi level. Binding energies are calculated with respect to the vacuum level. The vacuum level is found by summing the secondary electron cutoff and the photon energy (He I, $h\nu = 21.2$ eV). The valence band spectrum is shown in the ESI† as measured by UPS, showing the characteristic double peak of HOMO and HOMO-1 of C_{60}. For this data a smooth background function has been subtracted. A multiple Gaussian peak fit is performed on the data and the width (σ) and center (μ) of the peaks are found from the fit. We take the value of $\mu + 2\sigma$ as the onset of the HOMO (−5.45 eV). Therefore estimated LUMO of the **FSC11** could be derived to be −3.72 eV from the equation $E_{LUMO} = E_{HOMO} + E_g$ (eV).

AFM measurement

AFM and CP-AFM measurements were performed on a Bruker AFM Multimode MMAFM-2 equipped with a Peak Force TUNA Application Module (Bruker). Pure SAMs of **SC10** before exchange and mixed-monolayers of **FSC11** were characterized by AFM. While individual C_{60} cages could not be resolved Fig. S16† shows clear qualitative differences before and after exchange, but low roughnesses ($R_a \approx 1$ nm) and no signs of aggregation or other irregularities. See ESI† for details.

Acknowledgements

This is a publication by the FOM Focus Group 'Next Generation Organic Photovoltaics', participating in the Dutch Institute for Fundamental Energy Research (DIFFER). R. C. C. and Y. Z. also acknowledge the European Research Council for the ERC Starting Grant 335473 (MOLECSYNCON).

References

1 A. Aviram and M. A. Ratner, *Chem. Phys. Lett.*, 1974, **29**, 277–283.
2 H. Ashwell, J. Bonham and L. Lyons, *Aust. J. Chem.*, 1980, **33**, 1619–1623.
3 A. Martin, J. Sambles and G. Ashwell, *Phys. Rev. Lett.*, 1993, **70**, 218.
4 A. Ulman, *Chem. Rev.*, 1996, **96**, 1533–1554.
5 C. Kaes, A. Katz and M. W. Hosseini, *Chem. Rev.*, 2000, **100**, 3553–3590.
6 T. Xu, I. R. Peterson, M. Lakshmikantham and R. M. Metzger, *Angew. Chem., Int. Ed.*, 2001, **40**, 1749–1752.
7 M.-K. Ng and L. Yu, *Angew. Chem., Int. Ed.*, 2002, **41**, 3598–3601.
8 A. Troisi and M. A. Ratner, *J. Am. Chem. Soc.*, 2002, **124**, 14528–14529.
9 R. McCreery, J. Dieringer, A. O. Solak, B. Snyder, A. M. Nowak, W. R. McGovern and S. DuVall, *J. Am. Chem. Soc.*, 2003, **125**, 10748–10758.
10 R. M. Metzger, *Chem. Rev.*, 2003, **103**, 3803–3834.
11 A. Troisi and M. A. Ratner, *Nano Lett.*, 2004, **4**, 591–595.
12 G. J. Ashwell, W. D. Tyrrell and A. J. Whittam, *J. Am. Chem. Soc.*, 2004, **126**, 7102–7110.
13 A. Honciuc, A. Jaiswal, A. Gong, K. Ashworth, C. W. Spangler, I. R. Peterson, L. R. Dalton and R. M. Metzger, *J. Phys. Chem. B*, 2005, **109**, 857–871.
14 J. C. Love, L. A. Estroff, J. K. Kriebel, R. G. Nuzzo and G. M. Whitesides, *Chem. Rev.*, 2005, **105**, 1103–1170.
15 G. J. Ashwell and A. Mohib, *J. Am. Chem. Soc.*, 2005, **127**, 16238–16244.
16 R. L. McCreery, J. Wu and R. P. Kalakodimi, *Phys. Chem. Chem. Phys.*, 2006, **8**, 2572–2590.
17 G. Ho, J. R. Heath, M. Kondratenko, D. F. Perepichka, K. Arseneault, M. Pézolet and M. R. Bryce, *Chem.–Eur. J.*, 2005, **11**, 2914–2922.
18 G. J. Ashwell and A. Chwialkowska, *Chem. Commun.*, 2006, 1404–1406.
19 G. J. Ashwell, B. Urasinska and W. D. Tyrrell, *Phys. Chem. Chem. Phys.*, 2006, **8**, 3314–3319.
20 N. Armstrong, R. C. Hoft, A. McDonagh, M. B. Cortie and M. J. Ford, *Nano Lett.*, 2007, **7**, 3018–3022.
21 E. A. Weiss, G. K. Kaufman, J. K. Kriebel, Z. Li, R. Schalek and G. M. Whitesides, *Langmuir*, 2007, **23**, 9686–9694.
22 X. Chen, S. Yeganeh, L. Qin, S. Li, C. Xue, A. B. Braunschweig, G. C. Schatz, M. A. Ratner and C. A. Mirkin, *Nano Lett.*, 2009, **9**, 3974–3979.
23 C. A. Nijhuis, W. F. Reus, J. R. Barber, M. D. Dickey and G. M. Whitesides, *Nano Lett.*, 2010, **10**, 3611–3619.
24 R. C. Chiechi, E. A. Weiss, M. D. Dickey and G. M. Whitesides, *Angew. Chem.*, 2008, **120**, 148–150.
25 Y. Zhang, Z. Zhao, D. Fracasso and R. C. Chiechi, *Isr. J. Chem.*, 2014, **54**, 513–533.
26 C. A. Nijhuis, W. F. Reus and G. M. Whitesides, *J. Am. Chem. Soc.*, 2009, **131**, 17814–17827.

27 C. A. Nijhuis, W. F. Reus and G. M. Whitesides, *J. Am. Chem. Soc.*, 2010, **132**, 18386–18401.
28 K. S. Wimbush, W. F. Reus, W. G. van der Wiel, D. N. Reinhoudt, G. M. Whitesides, C. A. Nijhuis and A. H. Velders, *Angew. Chem., Int. Ed.*, 2010, **49**, 10176–10180.
29 W. F. Reus, M. M. Thuo, N. D. Shapiro, C. A. Nijhuis and G. M. Whitesides, *ACS Nano*, 2012, **6**, 4806–4822.
30 N. Nerngchamnong, L. Yuan, D.-C. Qi, J. Li, D. Thompson and C. A. Nijhuis, *Nat. Nanotechnol.*, 2013, **8**, 113–118.
31 L. Yuan, N. Nerngchamnong, L. Cao, H. Hamoudi, E. del Barco, M. Roemer, R. K. Sriramula, D. Thompson and C. A. Nijhuis, *Nat. Commun.*, 2015, **6**, 6324.
32 A. R. Garrigues, L. Yuan, L. Wang, E. R. Mucciolo, D. Thompon, E. del Barco and C. A. Nijhuis, *Sci. Rep.*, 2016, **6**, 26517.
33 L. Cao, M. Yang, L. Yuan, N. Nerngchamnong, Y.-P. Feng, A. T. Wee, D.-C. Qi and C. A. Nijhuis, *J. Phys.: Condens. Matter*, 2016, **28**, 094006.
34 A. R. Garrigues, L. Wang, E. del Barco and C. A. Nijhuis, *Nat. Commun.*, 2016, **7**, 11595.
35 H. J. Yoon, K. C. Liao, M. R. Lockett, S. W. Kwok, M. Baghbanzadeh and G. M. Whitesides, *J. Am. Chem. Soc.*, 2014, **136**, 17155–17162.
36 L. Yuan, L. Jiang, D. Thompson and C. A. Nijhuis, *J. Am. Chem. Soc.*, 2014, **136**, 6554–6557.
37 L. Jiang, L. Yuan, L. Cao and C. A. Nijhuis, *J. Am. Chem. Soc.*, 2014, **136**, 1982–1991.
38 G. D. Kong, M. Kim, S. J. Cho and H. J. Yoon, *Angew. Chem., Int. Ed.*, 2016, **55**, 10307–10311.
39 L. Yuan, R. Breuer, L. Jiang, M. Schmittel and C. A. Nijhuis, *Nano Lett.*, 2015, **15**, 5506–5512.
40 S. Bosi, T. Da Ros, G. Spalluto and M. Prato, *Eur. J. Med. Chem.*, 2003, **38**, 913–923.
41 J.-F. Nierengarten, *New J. Chem.*, 2004, **28**, 1177–1191.
42 Y. He and Y. Li, *Phys. Chem. Chem. Phys.*, 2011, **13**, 1970–1983.
43 L. Rincón-García, A. K. Ismael, C. Evangeli, I. Grace, G. Rubio-Bollinger, K. Porfyrakis, N. Agraït and C. J. Lambert, *Nat. Mater.*, 2016, **15**, 289–293.
44 C. Zeng, H. Wang, B. Wang, J. Yang and J. Hou, *Appl. Phys. Lett.*, 2000, **77**, 3595.
45 C. A. Martin, D. Ding, J. K. Sørensen, T. Bjørnholm, J. M. van Ruitenbeek and H. S. van der Zant, *J. Am. Chem. Soc.*, 2008, **130**, 13198–13199.
46 D. Bonifazi, O. Enger and F. Diederich, *Chem. Soc. Rev.*, 2007, **36**, 390–414.
47 K. Kelly, Y.-S. Shon, T. Lee and N. Halas, *J. Phys. Chem. B*, 1999, **103**, 8639–8642.
48 P. Sudeep, B. I. Ipe, K. G. Thomas, M. George, S. Barazzouk, S. Hotchandani and P. V. Kamat, *Nano Lett.*, 2002, **2**, 29–35.
49 P. Peumans and S. Forrest, *Appl. Phys. Lett.*, 2001, **79**, 126–128.
50 W. B. Caldwell, K. Chen, C. A. Mirkin and S. J. Babinec, *Langmuir*, 1993, **9**, 1945–1947.
51 X. Shi, W. B. Caldwell, K. Chen and C. A. Mirkin, *J. Am. Chem. Soc.*, 1994, **116**, 11598–11599.
52 R. R. Sahoo and A. Patnaik, *J. Colloid Interface Sci.*, 2003, **268**, 43–49.
53 L. Grüter, F. Cheng, T. T. Heikkilä, M. T. González, F. Diederich, C. Schönenberger and M. Calame, *Nanotechnology*, 2005, **16**, 2143.
54 Y. Shirai, L. Cheng, B. Chen and J. M. Tour, *J. Am. Chem. Soc.*, 2006, **128**, 13479–13489.
55 Y. Shirai, J. M. Guerrero, T. Sasaki, T. He, H. Ding, G. Vives, B.-C. Yu, L. Cheng, A. K. Flatt, P. G. Taylor, *et al.*, *J. Org. Chem.*, 2009, **74**, 7885–7897.
56 M. del Carmen Gimenez-Lopez, M. T. Räisänen, T. W. Chamberlain, U. Weber, M. Lebedeva, G. A. Rance, G. A. D. Briggs, D. Pettifor, V. Burlakov, M. Buck, *et al.*, *Langmuir*, 2011, **27**, 10977–10985.
57 S. Chase, W. Bacsa, M. Mitch, L. Pilione and J. Lannin, *Phys. Rev. B: Condens. Matter Mater. Phys.*, 1992, **46**, 7873.
58 E. I. Altman and R. J. Colton, *Surf. Sci.*, 1993, **295**, 13–33.
59 M. Hunt, S. Modesti, P. Rudolf and R. Palmer, *Phys. Rev. B: Condens. Matter Mater. Phys.*, 1995, **51**, 10039.
60 C.-T. Tzeng, W.-S. Lo, J.-Y. Yuh, R.-Y. Chu and K.-D. Tsuei, *Phys. Rev. B: Condens. Matter Mater. Phys.*, 2000, **61**, 2263.
61 L. A. Bumm, J. J. Arnold, M. T. Cygan, T. D. Dunbar, T. P. Burgin, L. Jones, D. L. Allara, J. M. Tour and P. S. Weiss, *Science*, 1996, **271**, 1705–1707.
62 D. Thompson and C. A. Nijhuis, *Acc. Chem. Res.*, 2016, **49**, 2061–2069.
63 L. Yuan, D. Thompson, L. Cao, N. Nerngchangnong and C. A. Nijhuis, *J. Phys. Chem. C*, 2015, **119**, 17910–17919.
64 T. W. Kelley, E. Granstrom and C. D. Frisbie, *Adv. Mater.*, 1999, **11**, 261–264.
65 O. E. Castañeda Ocampo, P. Gordiichuk, S. Catarci, D. A. Gautier, A. Herrmann and R. C. Chiechi, *J. Am. Chem. Soc.*, 2015, **137**, 8419–8427.
66 S. Kumar, J. T. van Herpt, R. Y. Gengler, B. L. Feringa, P. Rudolf and R. C. Chiechi, *J. Am. Chem. Soc.*, 2016, **138**, 12519–12526.
67 H. M. Saavedra, C. M. Barbu, A. A. Dameron, T. J. Mullen, V. H. Crespi and P. S. Weiss, *J. Am. Chem. Soc.*, 2007, **129**, 10741–10746.
68 S. Patole, C. Baddeley, D. O'Hagan and N. Richardson, *J. Phys. Chem. C*, 2008, **112**, 13997–14000.
69 V. V. Tsukruk, L. M. Lander and W. J. Brittain, *Langmuir*, 1994, **10**, 996–999.
70 W. Li, J. A. Virtanen and R. M. Penner, *J. Phys. Chem.*, 1994, **98**, 11751–11755.

